Heating of Thin Foils with a Relativistic-Intensity Short-Pulse Laser

P. Audebert,[1] R. Shepherd,[2] K. B. Fournier,[2] O. Peyrusse,[3] D. Price,[2] R. Lee,[2] P. Springer,[2] J.-C. Gauthier,[1] and L. Klein[4]

[1]*Laboratoire pour l'Utilisation des Lasers Intenses (LULI), UMR 7605, CNRS-CEA, Université Paris VI-École Polytechnique, 91128 Palaiseau, France*

[2]*Lawrence Livermore National Laboratory, University of California, Livermore, California 94550*

[3]*Commisariat á l'Energie Atomique, BP 12, 91680 Bruyères-le-Châtel, France*

[4]*Department of Physics and Astronomy, Howard University, Washington, D.C. 20059*

(Received 5 October 2001; published 11 December 2002)

K-shell x-ray spectroscopy of sub-100 nm Al foils irradiated by high contrast, spatially uniform, 150 fs, $I\lambda^2 = 2 \times 10^{18}$ W μm^2/cm^2, laser pulses is obtained with 500 fs time resolution. Two distinct phases occur: At $\leq$ 500 fs a broad feature comparable to the resonance transitions occurs due to satellites, and at $\geq$ 500 fs the resonance transitions dominate. Initial satellites arise from a large area, high density, low temperature ($\sim$ 100 eV) plasma created by fast electrons. Thus, contrary to predictions, a short, high intensity laser incident on a thin foil does not create a uniform, hot dense plasma.

DOI: 10.1103/PhysRevLett.89.265001 PACS numbers: 52.50.Jm, 52.25.Os, 52.70.La

Using detailed spectroscopic analysis of the K-shell emission, we present an investigation of the energy deposition and subsequent heating mechanism of an ultrathin aluminum foil, subjected to a high intensity, ultrashort laser pulse. This research differs from previous studies in that we simultaneously use a shorter time resolution (500 fs), a larger crystal x-ray spectrometer energy range (400 eV), and a higher, relativistic, laser intensity (10^{19} W/cm^2) with better control and management of the laser pulse energy contrast. These improvements have enabled us to obtain information that extends and sometimes contradicts previous ideas on the mechanisms involved in the dynamics of the plasma heating.

Studies of the x-ray spectrum emitted from a solid target heated with a short laser pulse with fast time resolution have a long history. The early experiments were performed with ps laser pulses and time resolution [1]. More recent studies make use of optical 100 fs pulses, amplified to $\geq$ 100 mJ, yielding focused intensities $> 10^{18}$ W/cm^2 [2]. With high contrast pulses, such intensities can be used to heat solid materials to elevated temperatures with minimal hydrodynamic expansion, producing a high energy density state for a short period of time, and yielding matter ideal for the study of the dynamics of hot and dense plasmas.

In the past, P-polarized laser light, focused on a solid target, was commonly used to increase the energy coupling through resonance absorption. For thick targets this produced large spatial gradients in the overdense interaction region due to the suprathermal electrons depositing their energy deep inside the target [3]. The resulting x-ray emission is produced by a plasma with large spatial temperature and density gradients. Although x-ray emission from these plasmas has been observed with ps resolution streak cameras [4,5], the measured spectra did not differ markedly from those of experiments using time-integrated x-ray diagnostics.

Experiments using sub-100 nm aluminum foil targets minimize the problems associated with temperature gradients. With foil thickness much smaller than the thermal penetration depth [4], the target is heated uniformly at constant density along the laser axis, as electron conduction propagates laser heating over the foil thickness before significant hydrodynamic motion can occur. Experimental studies [6] have compared the time scale for the evolution of K-shell x-ray emission to the cooling rate that is controlled by hydrodynamic plasma expansion. Later studies on thin foils with sub-ps time resolution, focused on the time history of the emission in the He_α spectral region and the effect of the laser pulse duration [7]. Satellites of He_α were observed with ps time resolution. It is not possible to compare the results of this experiment with the present work because of the larger time resolution and the smaller wavelength range covered.

The experiments to be described here were performed at the Lawrence Livermore National Laboratory USP laser facility [8]. The laser employed is a Ti:sapphire oscillator, utilizing chirped pulse amplification to generate high energy 150 fs duration pulses. The pulses are compressed in a vacuum compressor, frequency-doubled with a 1.5 μm thick KDP crystal, and focused on target with an $f/3.5$ off-axis parabola. The experiments use a 22.5° angle of incidence relative to target normal, chosen for alignment and to protect the laser chain. The peak intensity, required to obtain sufficient signal in the wide spectral range, is 10^{19} W/cm^2 ($I\lambda^2 \approx 2 \times 10^{18}$ W μm^2/cm^2). To minimize resonance absorption, *S*-polarized light is utilized.

The measured energy on target is in the range, 150–200 mJ at a wavelength of 400 nm and can be focused to a full-width at half maximum (FWHM) spot size of 2 μm. Equivalent target plane images indicate that 53% of the laser energy was located in the $1/e^2$ central spot. Since the crystal images the plasma on the slit without

magnification, the spatial resolution of the streak camera is defined by the 150 μm entrance slit that is larger than the laser focal spot.

Several diagnostics were used to monitor the high contrast, high intensity pulses and suppress any prepulse or pedestal from regenerative amplification. For each shot, the oscillator pulse spectrum was checked by imaging the zero order reflection from the grating into a spectrometer. To minimize the probability of a pulse with temporal "wings" being used in the experiment, pulses deviating more than 10% from the initial 100 fs Gaussian pulse spectrum were prevented from further amplification. The phase of the pulse also was monitored with a frequency resolved optical gate (FROG) system [9], and data from poorly compressed pulses were rejected. To suppress ASE the pulses were frequency doubled to 400 nm. No damage was observed when an unseeded pulse was focused on the 25 nm foil target, indicating that focused ASE, if present, produces no measurable effect. A high dynamic range autocorrelation measurement performed on the 800 nm fundamental pulse indicated an intensity contrast of $I_{\text{background}}/I_{\text{peak}} \approx 10^{-5}$ at 1.5 ps before the laser pulse peak, which is squared by frequency doubling. A low-dynamic range (10^{-4}), single shot autocorrelation was performed to monitor the pulse width. Also, a measurement of the contrast between the pulse and the prepulse due to leakage of the regenerative amplifier was performed and found to be less than 10^{-12}. Further, no transmitted energy was measured behind the targets during the shots, while energy on target was measured with a calorimeter.

The x rays were collected with a 500 fs time-resolution streak camera coupled to a dual-crystal von Hamòs x-ray spectrograph (see Fig. 1). The entrance slit of the *in vacuo* streak camera lies along the focusing axis of the crystals. Two RbAP crystals were bent to 3.6 and 3.0 cm radii to collect, in a single shot, simultaneous time-resolved data from He-like ions in the spectral region that includes the following: the $1s^2$-$1s2p$, He_α transition; and the $1s^2$-$1s3p$; He_β, $1s^2$-$1s4p$, He_γ transitions, respectively, and the associated satellite line transitions.

The spectra were focused onto the 25.4 mm long, 150 μm wide entrance slit of the streak camera. The transit time difference of x rays at different wavelengths, reflected off a single crystal, was used to calibrate and check the linearity of the sweep for each shot. Because of the high streak camera sweep-speed (2.6 ps/mm), the transit time difference for x rays reflecting off the two crystals produced a spatial gap between the streaked data from the respective crystals. In Fig. 1, the data for the case of a 150 fs, 2×10^{19} W/cm^2 laser pulse incident on a 500 Å thick Al foil target is displayed as a function of the streak camera sweep time. Both traces are inclined because of the time delay between low and high energy photons.

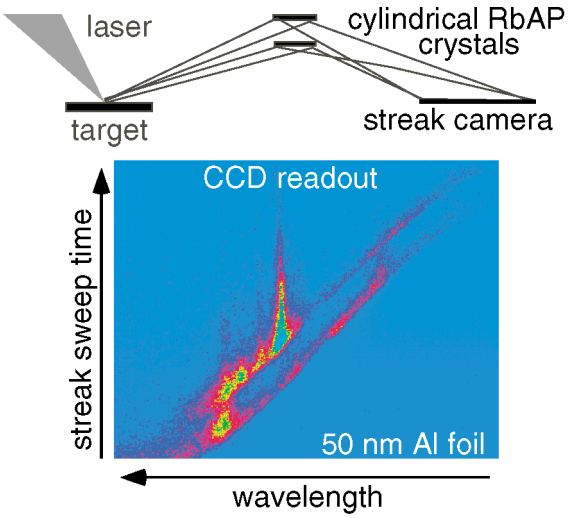

FIG. 1 (color). Experimental setup of the laser focusing and dual crystal x-ray collection. Typical data obtained for a 2×10^{19} W/cm^2, 150 fs pulse incident on a 50 nm Al foil. The upper trace shows the He_α line transition and Li-like dielectronic satellites. The lower trace shows the He_β and He_γ transitions.

The streaked data were intensified and collected with an ITT image intensifier mated to a 1024×1024 CCD camera. The x rays emitted with energies between 10 keV and 1 MeV were characterized using a scintillator/diode array. Twelve filtered photomultipliers were used for detection above 30 keV, and six filtered x-ray diodes were used for detection below that energy. To allow a reconstruction of the spectrum, the filters were chosen to provide seven data points from 100 to 500 keV. These points could be fitted with good reproducibility to a Maxwellian described by a temperature of 120 to 200 keV depending on the laser energy.

The intensity data of Fig. 1 are presented again in Fig. 2 in a plot of x-ray wavelength vs target arrival time. The spectra are corrected for streak camera CsI photocathode response, image intensifier gain, different solid angles of

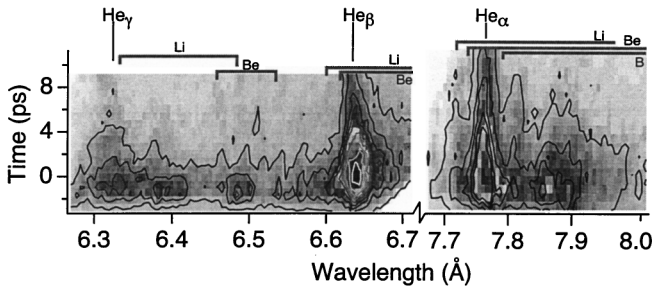

FIG. 2. Time resolved data for the same conditions as Fig. 1. The time axis here is that of the x-ray arrival time at the target. The entire spectrum from He_α to He_γ is displayed in one data record. The resonance transitions and dielectronic satellites are marked on the trace.

the crystal x-ray reflection, and time difference related to the different path lengths. The positions of the He-like resonance lines and their associated Li, Be, and B-like satellites have been identified in the figure. The lineouts analyzed in the following are taken from this corrected data.

Spectra over the range He_γ to He_β of the time-resolved data of Fig. 2 are presented in Fig. 3. The initial and peak emission spectra, as well as the background noise, are displayed, correctly scaled in intensity. The initial spectrum is recorded over the first 500 fs, starting at the time emission exceeded the background, and the peak emission data is taken 3 ps later. In addition, the time-integrated data is presented for comparison. It is to be emphasized that the features observed in the initial spectrum are reproducible and well above the background level.

The initial quasicontinuous spectrum seen between the two He lines is satellite line emission originating from doubly excited $1s2l4l'$ levels [6,10]. The integrated intensity of these lines is comparable to that of the resonance line intensity (~ 0.2 of He_β). At the onset of emission, He_β and He_γ appear as broad features and only later emerge as the narrow lines seen in the peak emission and time-integrated data. Previous experimental emission spectra of similar near-solid density, sub-100 nm foils, with ps time resolution can be found, for example, in Refs. [7,11], and are in agreement with the time-integrated spectrum of Fig. 3. We note that the He_α line near 7.76 Å in Fig. 2 also exhibits strong satellite emission at early time.

Independent of hydrodynamic simulations or kinetics calculations, the evolution of the initial satellite-resonance line intensity distribution can be understood as follows: At early time (< 500 fs) the plasma has not expanded so that the ions remain at solid density [6] with

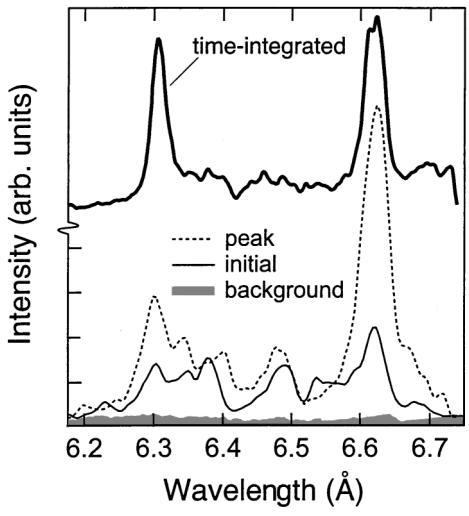

FIG. 3. Spectral lineout of the Fig. 2 trace in the region from He_γ to He_β. Note that the lower three traces are correctly scaled, but the time integrated data has been shifted for clarity.

LTE ion state populations. The initial laser energy deposition creates core ionization of the Al in a cylindrical volume defined by the laser spot and the foil thickness. Then, from the early time He_β to He_γ line intensity ratio, we can estimate the temperature of the laser spot to be ~keV. If we were to assume that all the emission arises from this hot, uniform-temperature (keV) laser spot then the LTE population ratios are such that resonance lines and satellites could not be emitted with the intensity ratio observed. Because of the high temperature of the laser spot, an insufficient number of ions are created in states that radiate satellite lines relative to those that radiate resonance lines. A second spatially distinct low temperature plasma that will emit satellite and resonance lines with comparable intensities is required. Thus, a large volume, cool ($\sim$ 100 eV) plasma created simultaneously with the hot laser spot explains the observed satellite to He_β intensity ratio of 0.2.

A more accurate calculation can be performed using non-LTE population kinetics to provide details for the above simple model. The initial laser energy deposition that creates core ionization of the Al in the laser spot volume results in: (a) hot electrons at the quiver energy (150 keV); (b) Auger electrons (~ keV); and (c) low energy electrons (eV) from the valence shell. With a kinetics model for the early time He_β to He_γ line intensity ratio, we estimate the temperature of the laser spot to be 1500 eV. This calculation is in accord with a hydrodynamic simulation that replaces the laser field with an initial foil temperature to compute the experimental He_β and He_γ emission history. To obtain comparable intensities of the He_β line and the associated satellites, kinetics calculations for solid density matter indicate that a plasma temperature of 150 eV will maximize this ratio. From the relative populations of ions radiating He_β to those radiating satellites at this temperature, an estimate of the size of the cool plasma, relative to the hot laser spot plasma can be made. For the observed total satellite intensity to be 0.2 of the total resonance line intensity, at solid density the150 eV plasma must be ≥ 25 times the volume of the 1500 eV plasma. The cool plasma, thus, has a radius 5 times the radius of the hot laser spot. Changes in the temperature estimates by $\pm 30\%$ do not alter these conclusions.

The physical mechanism for the creation of the two distinct temperature regions also can be understood by a simple physical picture. A large population of hot electrons with mean free path much larger than the focal spot is created in the laser spot by laser field acceleration. Because of the larger mass of the ions, the initial energy acquired by these hot electrons produces a charge separation, resulting in a large electrostatic field that causes a return current. The hot electrons on return to the target heat a large area of the foil, generating inner shell vacancies and Auger decay that increases the population of doubly excited states. After the transfer of energy to the

solid density matter, the hot electron energy is on the order of tens of keV [12]. The temperature equilibrates with a relaxation time given by $\tau_{ee} \approx (1.3 \times 10^5/n_e\lambda_{ee})(T_{\rm hot} + T_e)^{3/2}$, where λ_{ee} is the Coulomb logarithm, yielding τ_{ee} of a few 100 fs for solid density matter at $T_e \sim 100$ eV [10]. Therefore, after the laser pulse, the hot electrons thermalize and a radial temperature gradient exists in the foil with 1500 eV at the central laser spot and 150 eV in surrounding region. This time evolution mechanism is consistent with data from the hard x-ray scintillator/diode array indicating a large fraction of the absorbed laser energy produces hot electrons [13]. Further, there are indications our picture is in accord with recent PIC simulations [14], and with analyses performed with hydrodynamic simulation, post-processed by a collisional-radiative code [15].

In summary, we have performed a spectroscopic analysis of the K-shell emission from an Al plasma created from ultrathin foils heated with a relativistic intensity, ultrashort pulse laser. Our work addresses some of the difficulties encountered in previous attempts to model the temporal behavior of thin foil emission by detailed atomic physics [6]. The small foil thickness used in the present experiments minimizes longitudinal thermal gradients and permits a simple interpretation of the data.

Since the x-ray instrumentation used did not provide spatially resolved data, the spatial information was inferred. Data that is not spatially integrated could be obtained using a dot target, or optical probes might be useful [16]. This x-ray spectroscopic experiment is part of a continuing effort to investigate the dynamics of extreme states of matter, and we have shown here that producing very hot dense matter with lasers is not as straightforward as supposed previously. To deposit a given amount of energy in the target before hydrodynamic motion occurs, short pulses are required. But, for the same energy content, shorter pulse durations result in higher laser intensities, and that implies larger electron quiver velocities. These hot electrons are then responsible for a delocalized energy deposition, creating a low temperature, large volume plasma. The possibility of producing a high density, hot plasma by a very short pulse, high intensity laser requires further study.

The authors would like to thank Jean-Paul Geindre for numerous and helpful discussions. We acknowledge the invaluable support of the USP technical staff at LLNL. This work was performed under the auspices of the U.S. DoE, by University of California, LLNL, under Contract No. W-7405-Eng-48. Partial support was also provided by DoE HEDS Grant No. DE-FG03-98DP00213 to Howard University.

[1] P. Gibbon and E. Förster, Plasma Phys. Controlled Fusion **38**, 769 (1966); R. Falcone and M. Murnane, in *Short Wavelength Coherent Radiation*, AIP Conf. Proc. No. 147 (AIP, New York, 1986), p. 81.

[2] M. Murnane, H. Kapteyn, and R. Falcone, Phys. Rev. Lett. **62**, 155 (1989); Appl. Phys. Lett. **56**, 1948 (1990); S. Gordon *et al.*, Opt. Lett. **XX**, 484 (1993); P. Audebert *et al.*, J. Phys. B **27**, 3303 (1994); J. Kieffer *et al.*, J. Opt. Soc. Am. B **13**, 133 (1996); J. Larsson *et al.*, Opt. Lett. **22**, 1012 (1997); J.-C. Gauthier *et al.*, Phys. Plasmas **4**, 1811 (1997); D. Altenbernd *et al.*, J. Phys. B **30**, 3969 (1997); C. Côté *et al.*, J. Phys. B **31**, L883 (1998); A. Saemann *et al.*, Phys. Rev. Lett. **82**, 4843 (1999); K. Eidmann *et al.*, J. Quant. Spectrosc. Radiat. Transfer **65**, 173 (2000); U. Andiel *et al.*, Phys. Rev. E **63**, 26407 (2001).

[3] J. Matte *et al.*, Phys. Rev. Lett. **72**, 1208 (1994); F. Beg *et al.*, Phys. Plasmas **4**, 447 (1997); F. Rosmej, J. Phys. B **30**, L819 (1997).

[4] C. Y. Côté, J. C. Kieffer, and O. Peyrusse, Phys. Rev. E **56**, 992 (1997).

[5] K. Eidmann *et al.*, in *Atomic Processes in Plasmas*, edited by R. Mancini and R. Phaneuf, AIP Conf. Proc. No. 547 (AIP, New York, 2000), p. 238.

[6] R. Shepherd *et al.*, J. Quant. Spectrosc. Radiat. Transfer **58**, 911 (1997); T. Kato *et al.*, J. Quant. Spectrosc. Radiat. Transfer **58**, 661 (1997).

[7] P. Gallant *et al.*, J. Quant. Spectrosc. Radiat. Transfer **65**, 243 (1999).

[8] W. E. White *et al.*, Opt. Lett. **17**, 1067 (1992)

[9] D. Kane and R. Trebino, IEEE J. Quantum Electron. **29**, 571 (1993).

[10] A. Yamaguchi and J. Nizui, Phys. Lett. A **72**, 333 (1979).

[11] J. Fuchs *et al.*, Phys. Plasmas **6**, 2569 (1999).

[12] S. Weber, G. Bonnaud, and J.-C. Gauthier, Phys. Plasmas **8**, 387 (2001); Y. Sentoku, K. Mima, T. Taguchi , S. Miyamoto, and Y. Kishimoto, Phys. Plasmas **5**, 4366 (1998); Y. Sentoku *et al.*, Phys. Rev. E **62**, 7271 (2000).

[13] W. Lawson, P. Rambo, and D. Larson, Phys. Plasmas **4**, 788 (1997); G. Malka, E. Lefebvre, and J. Miquel, Phys. Rev. Lett. **78**, 3314 (1997).

[14] A. Zhidkov and A. Sasaki, Phys. Plasmas **7**, 1341 (2000).

[15] K. Eidmann, J. Meyer-ter-Vehn, T. Schlegel, and S. Hüller, Phys. Rev. E **62**, 1202 (2000).

[16] A. Forsman *et al.*, Phys. Rev. E **58**, R1248 (1998)